Large inverse spin Hall effect in the antiferromagnetic metal Ir$_{20}$Mn$_{80}$

J. B. S. Mendes,[1] R. O. Cunha,[1] O. Alves Santos,[1] P. R. T. Ribeiro,[1] F. L. A. Machado,[1]
R. L. Rodríguez-Suárez,[2] A. Azevedo,[1] and S. M. Rezende[1,*]

[1]*Departamento de Física, Universidade Federal de Pernambuco, 50670-901, Recife, PE, Brasil*
[2]*Facultad de Física, Pontificia Universidad Católica de Chile, Casilla 306, Santiago, Chile*

A spin current is usually detected by converting it into a charge current through the inverse spin Hall effect (ISHE) in thin layers of a nonmagnetic metal with large spin-orbit coupling, such as Pt, Pd, and Ta. Here we demonstrate that Ir$_{20}$Mn$_{80}$, a high-temperature antiferromagnetic metal that is commonly employed in spin-valve devices, exhibits a large inverse spin Hall effect, as recently predicted theoretically. We present results of experiments in which the spin currents are generated either by microwave spin pumping or by the spin Seebeck effect in bilayers of singe-crystal yttrium iron garnet (YIG)/Ir$_{20}$Mn$_{80}$ and compare them with measurements in YIG/Pt bilayers. The results of both measurements are consistent, showing that Ir$_{20}$Mn$_{80}$ has a spin Hall angle similar to Pt, and that it is an efficient spin-current detector.

PACS number(s): 72.25.Mk, 75.70.Cn, 76.50.+g

The generation and detection of spin currents are key processes for investigating basic physics phenomena and for applications in the field of spintronics [1–3]. The two most used techniques to generate spin currents in hybrid magnetic structures employ the spin-pumping effect (SPE) [4–7] and the spin Seebeck effect [8–12]. The detection of a spin current is usually made by sensing the electric voltage associated with the charge current generated by means of the inverse spin Hall effect (ISHE) [7,12]. The ISHE is well established in normal metals (NM) with large spin-orbit coupling, such as Pt, Ta, and Pd, and intense efforts have been made to discover new spin-detector materials aiming at enlarging the possibilities of spintronics. Recently [13] is has been shown that ferromagnetic permalloy (Py) can also be used to detect spin currents generated by the longitudinal spin Seebeck effect (LSSE) with an efficiency similar to that in Pt. However, spin-pumping experiments [14] revealed that the interface exchange interaction with another ferromagnet (FM) produces a coupling in their excitation modes, thus limiting the ability of Py as a spin-current detector in phenomena involving magnetization dynamics.

Recently Chen *et al.* [15] have shown theoretically that IrMn$_3$, a high-temperature noncollinear antiferromagnet (AF) with zero net magnetization, has a large anomalous Hall conductivity. Although the calculation of Ref. [15] was done for the single-crystal γ phase of IrMn$_3$, one expects the existence of the same property in polycrystalline Ir$_{20}$Mn$_{80}$ (IrMn) since it is formed by grains of IrMn$_3$ [16,17]. Polycrystalline IrMn fabricated under an applied magnetic field has oriented grains and exhibits macroscopic AF order. It is commonly employed to pin an adjacent FM magnetization in spin-valve devices [18] through the interfacial exchange bias [19]. Since the origin of the spin Hall effect (SHE) is the same as the anomalous Hall effect [12], IrMn is then likely to exhibit large SHE and ISHE, which are key phenomena for spintronics. Testing this property is of current interest in view of the growing interest in using AF materials in spintronic applications [20–24]. One advantage of an AF as a spin detector, compared to

ferromagnetic Py, is that its excitation frequencies are far apart from those in a FM, so that their mode coupling is negligible. In this Rapid Communication we demonstrate that IrMn indeed exhibits a large ISHE and is an efficient detector of spin currents generated either by microwave spin pumping or by the longitudinal spin Seebeck effect.

The experiments reported here were carried out with bilayers made of the ferromagnetic insulator (FMI) yttrium iron garnet (YIG-Y$_3$Fe$_5$O$_{12}$) capped either with IrMn or Pt. The measurements in YIG/IrMn are compared with similar ones done with YIG/Pt because the latter has been well studied [25–37]. The two methods most widely used to generate spin currents in FMI/metallic layer (ML) structures are sketched in Fig. 1. Figure 1(a) illustrates the spin-pumping process, where the magnetization in the FMI layer is driven by a rf magnetic field with microwave frequency perpendicular to the static field H, in the configuration of the ferromagnetic resonance (FMR) experiments. The precessing magnetization $\vec{M}$ generates a spin current density at the FMI/ML interface given by $\vec{J}_S = (\hbar g_{\mathrm{eff}}^{\uparrow\downarrow}/4\pi M^2)(\vec{M} \times \partial\vec{M}/\partial t)$, where $g_{\mathrm{eff}}^{\uparrow\downarrow}$ is the real part of the effective spin mixing conductance at the interface that takes into account the spin-pumped and back-flow spin currents [4,5]. In the ML, the spin current formed by electrons with opposite spins moving in opposite directions, diffuses with a characteristic length given by the spin-flip diffusion length, which is on the order of a few nanometers in metals with large spin-orbit scattering. Then, as illustrated in Fig. 1, a fraction of the electrons undergoes spin-orbit scattering generating a transverse charge motion which has a current density $\vec{J}_C$ given by $\vec{J}_C = \theta_{\mathrm{SH}}(2e/\hbar)\vec{J}_S \times \vec{\sigma}$, where θ_{SH} is the spin Hall angle and $\vec{\sigma}$ is the spin polarization. This produces a voltage measured at the ends of the ML which is proportional to the spin-current density and the ML resistance. The use of insulating YIG as the ferromagnetic medium in spin-pumping experiments eliminates spurious effects that occur in metallic FM, such as the anisotropic magnetoresistance [25–30]. The second method we use to generate a spin current is based on the longitudinal spin Seebeck effect (LSSE), illustrated in Fig. 1(b). In this case, according to the model of Ref. [35], a thermal gradient applied across the thickness of the bilayer produces a bulk magnon

*Corresponding author: rezende@df.ufpe.br
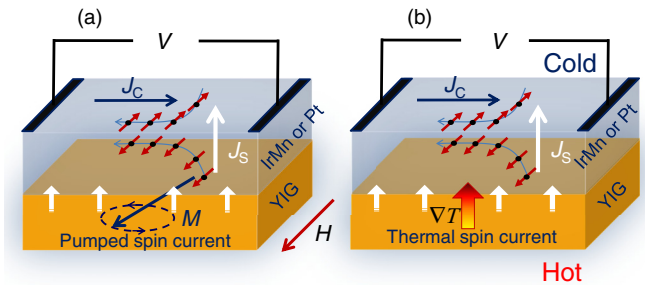
FIG. 1. (Color online) Sketches showing the YIG/IrMn or YIG/Pt structures and the electrodes used to measure the dc voltage due to the ISHE charge current in the metallic layer resulting from the spin currents generated in two configurations: (a) microwave FMR spin pumping and (b) longitudinal spin Seebeck effect. The static field H is applied in the film plane at an arbitrary angle with the sample edge.

spin current that results in a spin-pumped spin current across the FMI/ML interface proportional to the temperature gradient and to the spin-mixing conductance. The LSSE in FMI/NM bilayers is not contaminated by the Nernst effect [13,31–34].

In a spin-pumping experiment with a bilayer of a FMI layer in contact with a ML, a rf magnetic field with microwave frequency applied perpendicularly to the static field drives the magnetization precession of the excitation modes, the spin waves, or magnons. At the interface the precessing spins in the FM generate a spin-pumping spin current that flows into the ML producing two effects: (1) Increased damping of the magnetic excitation due to the flow of spin angular momentum out of the FM [4,5,36]; and (2) generation of a charge current by means of the ISHE that produces a voltage at the ends of the ML [6,7,25–30]. These two independent phenomena make it possible to extract material parameters from the measurements of the FMR absorption and the spin-pumping voltage.

The results of the measurement of the microwave FMR absorption are shown in Fig. 2. The sample is introduced through a small hole in the back wall of a rectangular microwave waveguide in a position of maximum microwave field h and zero rf electric field. This precaution avoids the generation of galvanic effects in the ML driven by the rf electric field. The waveguide is placed between the poles of an electromagnet of a homemade ferromagnetic resonance (FMR) spectrometer so that the static magnetic field with intensity H and the microwave field are in the film plane and kept perpendicular to each other as the sample is rotated. With this configuration we can investigate the angular dependence of the spectra. We use a shortened waveguide instead of a resonating microwave cavity to avoid detuning produced by the strong resonance of YIG and also nonlinear effects. By modulating the field at 1.2 kHz with a pair of Helmholtz coils and using lock-in detection, we obtain field scan spectra of the field derivative dP/dH of the microwave absorption lines. We have used two identical samples of single-crystal YIG films with thickness 6.0 μm, grown by liquid-phase epitaxy on 0.5 mm thick (111) gallium gadolinium garnet (GGG) substrate and cut in the form of rectangles with lateral dimensions 1.5×3.0 mm^2. Figure 2(a) shows the spectrum of one of the samples, measured with the static field in-plane and normal to the long direction, at a frequency $f = 9.4$ GHz and input microwave power 32 mW,
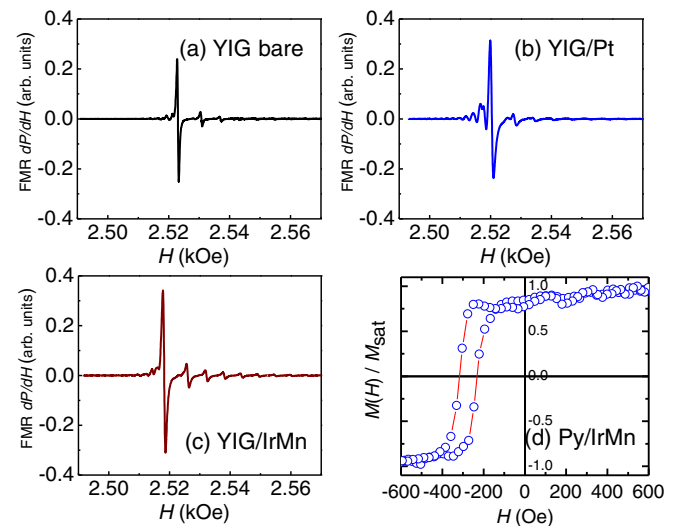
FIG. 2. (Color online) (a), (b), and (c) Field scan microwave FMR absorption derivative spectra at a frequency 9.4 GHz of 6 μm thick YIG film with lateral dimensions 1.5×3.0 mm^2 with the magnetic field applied in the film plane normal to the long dimension. In (a) the YIG film is bare while in (b) and (c) it is covered, respectively, with Pt (4 nm) and IrMn (5 nm). (d) Magneto-optical Kerr Effect (MOKE) magnetometry hysteresis loop of Py measured in Si(100)/Cu(8 nm)/Py(4 nm)/IrMn(4 nm) exhibiting the exchange bias effect produced by the AF arrangement of IrMn.

low enough to avoid nonlinear effects with the shortened waveguide setup. The spectrum in Fig. 2(a) obtained before deposition of a metallic layer on the YIG film allows a clear identification of the absorption lines. They correspond to standing spin-wave modes that have quantized in-plane wave numbers k due to the boundary conditions at the edges of the film [38–40]. The strongest line corresponds to the FMR mode that has frequency close to the spin wave with $k = 0$, given by $\omega_0 = \gamma(H + H_A)^{1/2}(H + H_A + 4\pi M + H_S)^{1/2}$, where $\gamma = 2\pi \times 2.8$ GHz/kOe for YIG, $4\pi M$ is the saturation magnetization (1.76 kG at room temperature), and H_A and H_S are, respectively, the in-plane and the out-of-plane (surface) anisotropy fields. The lines to the left of the FMR mode correspond to hybridized standing spin-wave surface modes, whereas those to the right are volume modes. All modes have a very similar peak-to-peak linewidth of 0.5 Oe, corresponding to a half-width at half-maximum (HWHM) of $\Delta H \approx 0.43$ Oe.

The bilayer samples were prepared by deposition of Pt (4 nm) and IrMn (5 nm) layers on the same two YIG film strips used for the FMR measurements by means of dc magnetron sputtering. In the deposition of the IrMn layer a field of 60 Oe was applied in the film plane and perpendicularly to the long strip dimension in order to orient the polycrystalline grains and produce the macroscopic AF arrangement. In attempts to characterize the AF arrangement of the IrMn layer by magnetometry in high fields, the much larger moment of the thick YIG film precludes any clear conclusion. So we have prepared a test sample of Si(100)/Cu(8 nm)/Py(4 nm)/IrMn(4 nm) under the same conditions of the YIG/IrMn bilayer in order to test the exchange bias of Py in contact with IrMn. Figure 2(d) shows the hysteresis loop of Py displaced in the field axis characterizing the exchange bias [19] and
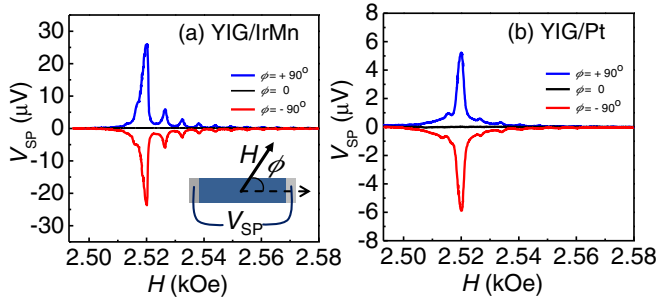
FIG. 3. (Color online) Field scan of the spin-pumping-ISHE voltage produced by FMR microwave excitation at a frequency 9.4 GHz in bilayers of YIG(6 μm)/IrMn(5 nm) in (a) and YIG(6 μm)/ Pt(4 nm) in (b). The measurements in (a) and (b) were done with a shortened waveguide and input power 80 mW. The inset in (a) shows a sketch of the electrodes and connections used to measure the dc voltage in the metal layer, with the static field H in the film plane at an angle ϕ with the sample axis.

consequently the AF arrangement of the IrMn layer. The contact of the metallic layer with the YIG film produces two noticeable effects on the microwave spectra, as shown in Figs. 2(b) and 2(c). First, all spectra shift uniformly to lower fields indicating that the metallic layer creates a surface anisotropy field. The other effect is the broadening of the lines due to the additional damping produced by the spin-pumping mechanism [4,5,36,41,42]. The broadening is nearly the same for all modes, their HWHM linewidths increase from 0.43 Oe in bare YIG to 0.68 Oe in YIG/IrMn and 1.0 Oe in YIG/Pt. Since the additional FMR linewidth due to spin-pumping damping is proportional to $g_{\mathrm{eff}}^{\uparrow\downarrow}$, the real part of the effective spin mixing conductance of the FMI/ML interface, one concludes from the data in Fig. 2 that $g_{\mathrm{eff}}^{\uparrow\downarrow}$ in YIG/IrMn is 2.3 times smaller than in YIG/Pt, which is in the range 10^{13}–10^{14} cm^{-2} [14,27–30].

For the investigation of the spin-pumping voltage V_{SP}, during the preparation of the samples, two 150 μm wide Ag strips were deposited at the ends of the metallic layers, to which copper thin wires were attached with silver paint, as illustrated in the inset of Fig. 3(a). The two wires were connected to a dc nanovoltmeter for a direct measurement of V_{SP}. The sample is mounted on the tip of a PVC rod and inserted in the hole of the shortened waveguide setup, so that it can be rotated while maintaining the static and rf fields in the plane and perpendicular to each other. The measurements are made at a fixed angle ϕ of the field relative to the long direction of the YIG/ML strip, without ac field modulation and with field sweep to obtain spectra of $V_{\mathrm{SP}}(H)$. Figure 3 shows the spectra of the spin-pumping voltage $V_{\mathrm{SP}}(H)$ measured at a frequency of 9.4 GHz and incident microwave power of 80 mW. Figures 3(a) and 3(b) for YIG/IrMn and YIG/Pt exhibit spectra containing lines corresponding to the same standing spin-wave modes of the absorption spectra in Fig. 2. The spin-pumping voltage has its origin in two combined processes, the spin-pumping mechanism [4,5] and the ISHE [7]. Since the charge current in the ML is proportional to the $\vec{J}_S \times \vec{\sigma}$ and the spin polarization is parallel to the static field, the spin pumping voltage V_{SP} vanishes when the field is along the film strip ($\phi = 0$), is finite and positive for $\phi = 90°$ and changes

sign when the field is reversed. The peak value of the spin-pumping-ISHE voltage at the FMR resonance field is $V_{\mathrm{SP}} \propto R_N \theta_{\mathrm{SH}} g_{\mathrm{eff}}^{\uparrow\downarrow} P / \Delta H^2$, where R_N is the resistance of the metallic layer, P is the microwave power, and ΔH is the linewidth of the FMR absorption [14,43–45]. The resistances measured between the two electrodes are $R_{\mathrm{Pt}} = 178$ Ω for Pt, consistent with the conductivity $\sigma_{\mathrm{Pt}} = 2.42 \times 10^4$ Ω^{-1} cm^{-1} [45], and $R_{\mathrm{IrMn}} = 1250$ Ω, consistent with the conductivity $\sigma_{\mathrm{IrMn}} = 3.6 \times 10^3$ Ω^{-1} cm^{-1} [46]. Using the results obtained from the FMR data in Fig. 2, $\Delta H_{\mathrm{IrMn}} = 0.68 \Delta H_{\mathrm{Pt}}$, $g_{\mathrm{IrMn}}^{\uparrow\downarrow} = 0.43 g_{\mathrm{Pt}}^{\uparrow\downarrow}$, and the voltage peak values in Fig. 3, $V_{\mathrm{IrMn}} \approx 5 V_{\mathrm{Pt}}$, we obtain a spin Hall angle for IrMn of $\theta_{\mathrm{SH-IrMn}} \approx 0.8 \theta_{\mathrm{SH-Pt}}$.

In order to confirm the spin Hall properties of IrMn we have done measurements with the longitudinal spin Seebeck effect (LSSE), in which the YIG/ML bilayer sample is subject to a temperature gradient normal to the plane [31–35]. We have used GGG/YIG/IrMn and GGG/YIG/Pt samples prepared in the same conditions as the ones used in the spin-pumping experiments but having larger lateral dimensions, 10×2.5 mm^2, to allow more room for the application of the temperature difference. The sketch of the sample mount is illustrated in the inset of Fig. 4(a). A commercial Peltier module is used to heat or cool the side of the metallic layer, while the other side of the sample is in thermal contact with a copper block maintained at room temperature. The temperature difference ΔT across the GGG/YIG/NM sample is measured using a differential thermocouple, with one junction attached to a thin copper strip placed between the Peltier module and the sample structure and the other to the copper block. Figures 4(a) and 4(c)
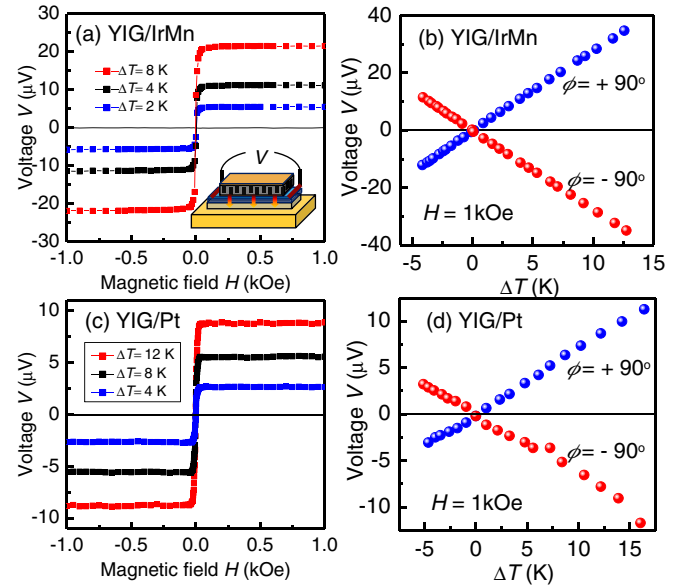
FIG. 4. (Color online) Variation of the ISHE voltage created by the longitudinal spin Seebeck effect with the temperature difference ΔT between the two sides of the samples under a magnetic field with intensity H applied in the plane transversely to the direction of the measured voltage. (a) and (c) Voltage as a function of H for YIG/IrMn and YIG/Pt for various values of ΔT. (b) and (d) Voltage as function of ΔT for $H = 1.0$ kOe in both directions. The inset in (a) shows the sketch of the GGG/YIG/ML sample mount with the Peltier module used to apply the temperature difference and the electrodes used to measure the dc voltage.

show the measured variation of the voltage with the intensity H of the magnetic field applied perpendicularly to the long sample dimension ($\phi = 90°$) for the YIG/IrMn and the YIG/Pt samples, respectively, for several values of the temperature difference ΔT. The change in the sign of the voltage with the reversal in the direction of the field is due to the change in the sign of the spin polarization. Figures 4(b) and 4(d) show the measured variation of the voltage, in both samples, with the temperature difference ΔT, for a field $H = 1$ kOe applied perpendicularly to the long strip direction, $\phi = \pm 90°$. Both data exhibit the well known linear variation with ΔT and sign change with the reversal of the field. Since YIG is an insulator, in both samples the voltage is entirely due to the spin Seebeck effect. According to the model of Ref. [35], the thermal gradient in the FMI layer creates a bulk magnon spin current that produces a spin-pumped spin current in the ML layer. This generates a charge current by means of the ISHE, resulting in a voltage at the ends of the ML layer $V \propto R_N \theta_{SH} g_{eff}^{\uparrow\downarrow} \Delta T$. Considering the measured resistances $R_{IrMn} = 3200$ Ω and $R_{Pt} = 314$ Ω and the average values of the voltages in Fig. 4 at the same temperature difference, $V_{IrMn} \approx 4 V_{Pt}$, we obtain the spin Hall angle for IrMn of $\theta_{SH\text{-}IrMn} \approx 0.8 \theta_{SH\text{-}Pt}$. This is the same value measured in the spin-pumping experiments, confirming that IrMn has a spin Hall angle similar to that of platinum. Considering that the voltage created by a spin current through the ISHE is proportional to the spin Hall angle and also to the resistance of the ML, one can define a figure of merit for a spin-current detector as the ratio θ_{SH}/σ_{ML}, where σ_{ML} is the ML conductivity. With this criterion IrMn has a figure of merit for spin-current detection 6.5 times larger than Pt, and similar to that of Ta, which was said to exhibit a giant spin Hall effect when discovered [47].

Finally, in order to test the correlation between the antiferromagnetism and the spin Hall properties of IrMn, we have also measured the microwave spin-pumping voltage in a YIG/IrMn bilayer with the same dimensions as the sample of Fig. 3(a) but prepared with no applied field during the deposition of the IrMn layer. In this case the IrMn layer is not textured and does not have macroscopic AF order. It turned out that the FMR and the $V_{SP}(H)$ spectra obtained in the same conditions described earlier were nearly identical to the ones in Figs. 2(c) and 3(a), revealing that in IrMn there is no correlation between the spin Hall properties and the macroscopic AF arrangement. This result is not completely unexpected. According to the theoretical model of Chen *et al.* [15], the origin of the anomalous Hall effect in IrMn$_3$ is based on two factors: First, the triangular arrangement of the magnetic moments in the AF sublattices breaks time-reversal symmetry; and second, the large spin-orbit coupling of the heavy Ir atoms is transferred to the magnetic Mn atoms by their hybridization. These occur locally and give rise to an intrinsic mechanism for the spin Hall effect, regardless of how grains of IrMn$_3$ are oriented in polycrystalline Ir$_{20}$Mn$_{80}$. The spin polarization of the electrons in the spin current is determined by the direction of the applied magnetic field and not by the macroscopic AF arrangement.

In summary, we have demonstrated that Ir$_{20}$Mn$_{80}$, a high-temperature antiferromagnetic metal that is commonly employed in spin-valve devices, exhibits spin Hall properties similar to that of platinum, confirming the theoretical prediction of Chen *et al.* [15]. Since the conductivity of Ir$_{20}$Mn$_{80}$ is almost one order of magnitude smaller than in Pt, the voltages generated in Ir$_{20}$Mn$_{80}$ by the ISHE are quite larger than in Pt, making this AF material a good candidate for a spin-current detector in spintronic applications.

[1] I. Zutic, J. Fabian, and S. Das Sarma, Rev. Mod. Phys. **76**, 323 (2004).

[2] S. Maekawa, S. O. Valenzuela, E. Saitoh, and T. Kimura (eds.), *Spin Current*, Series on Semiconductor Science and Technology (Oxford University Press, Oxford, 2012).

[3] E. Y. Tsymbal and I. Zutic (eds.), *Handbook of Spin Transport in Magnetism* (CRC Press, Boca Raton, FL, 2012).

[4] Y. Tserkovnyak, A. Brataas, and G. E. Bauer, Phys. Rev. Lett. **88**, 117601 (2002).

[5] Y. Tserkovnyak, A. Brataas, G. E. Bauer, and B. I. Halperin, Rev. Mod. Phys. **77**, 1375 (2005).

[6] A. Azevedo, L. H. Vilela Leão, R. L. Rodriguez-Suarez, A. B. Oliveira, and S. M. Rezende, J. Appl. Phys. **97**, 10C715 (2005).

[7] E. Saitoh, M. Ueda, H. Miyajima, and G. Tatara, Appl. Phys. Lett. **88**, 182509 (2006).

[8] K. Uchida, S. Takahashi, K. Harii, J. Ieda, W. Koshibae, K. Ando, S. Maekawa, and E. Saitoh, Nature (London) **455**, 778 (2008).

[9] K. Uchida, J. Xiao, H. Adachi, J. Ohe, S. Takahashi, J. Ieda, T. Ota, Y. Kajiwara, H. Umezawa, H. Kawai, G. E. W. Bauer, S. Maekawa, and E. Saitoh, Nat. Mater. **9**, 894 (2010).

[10] G. E. W. Bauer, E. Saitoh, and B. J. van Wees, Nat. Mater. **11**, 391 (2012).

[11] H. Adachi, K. Uchida, E. Saitoh, and S. Maekawa, Rep. Prog. Phys. **76**, 036501 (2013).

[12] J. E. Hirsh, Phys. Rev. Lett. **83**, 1834 (1999).

[13] B. F. Miao, S. Y. Huang, D. Qu, and C. L. Chien, Phys. Rev. Lett. **111**, 066602 (2013).

[14] A. Azevedo, O. Alves Santos, G. A. Fonseca Guerra, R. O. Cunha, R. Rodríguez-Suárez, and S. M. Rezende, Appl. Phys. Lett. **104**, 052402 (2014).

[15] H. Chen, Q. Niu, and A. H. MacDonald, Phys. Rev. Lett. **112**, 017205 (2014).

[16] T. Yamaoka, J. Phys. Soc. Jpn. **36**, 445 (1974).

[17] A. Kohn, A. Kovács, R. Fan, G. J. McIntyre, R. C. C. Ward, and J. P. Goff, Sci. Rep. **3**, 2412 (2013).

[18] S. S. P. Parkin *et al.*, J. Appl. Phys. **85**, 5828 (1999).

[19] J. Nogués and I. K. Schuller, J. Magn. Magn. Mater. **192**, 203 (1999).

[20] A. S. Núñez, R. A. Duine, P. Haney, and A. H. MacDonald, Phys. Rev. B **73**, 214426 (2006).

[21] A. B. Shick, S. Khmelevskyi, O. N. Mryasov, J. Wunderlich, and T. Jungwirth, Phys. Rev. B **81**, 212409 (2010).

[22] V. M. T. S. Barthem, C. V. Colin, H. Mayaffre, M.-H. Julien, and D. Givord, Nat. Commun. **4**, 2892 (2013).

[23] P. Merodio, A. Ghosh, C. Lemonias, E. Gautier, U. Ebels, M. Chshiev, H. Béa, V. Baltz, and W. E. Bailey, Appl. Phys. Lett. **104**, 032406 (2014).

[24] C. Hahn, G. de Loubens, O. Klein, M. Viret, V. V. Naletov, and J. Ben Youssef, arXiv:1310.6000.

[25] Y. Kajiwara, S. Takahashi, J. Ohe, K. Uchida, M. Mizuguchi, H. Umezawa, K. Kawai, K. Ando, K. Takanashi, S. Maekawa, and E. Saitoh, Nature (London) **464**, 262 (2010).

[26] C. W. Sandweg, Y. Kajiwara, K. Ando, E. Saitoh, and B. Hillebrands, Appl. Phys. Lett. **97**, 252504 (2010).

[27] L. H. Vilela-Leão, C. Salvador, A. Azevedo, and S. M. Rezende, Appl. Phys. Lett. **99**, 102505 (2011).

[28] K. Ando, T. Na, and E. Saitoh, Appl. Phys. Lett. **99**, 092510 (2011).

[29] V. Castel, N. Vlietstra, B. J. van Wees, and J. Ben Youssef, Phys. Rev. B **86**, 134419 (2012).

[30] C. Hahn, G. de Loubens, O. Klein, M. Viret, V. V. Naletov, and J. Ben Youssef, Phys. Rev. B **87**, 174417 (2013).

[31] K. Uchida, H. Adachi, T. Ota, H. Nakayama, S. Maekawa, and E. Saitoh, Appl. Phys. Lett. **97**, 172505 (2010).

[32] K. Uchida, T. Nonaka, T. Ota, H. Nakayama, and E. Saitoh, Appl. Phys. Lett. **97**, 262504 (2010).

[33] K. Uchida, T. Ota, H. Adachi, J. Xiao, T. Nonaka, Y. Kajiwara, G. E. W. Bauer, S. Maekawa, and E. Saitoh, J. Appl. Phys. **111**, 103903 (2012).

[34] T. Kikkawa, K. Uchida, Y. Shiomi, Z. Qiu, D. Hou, D. Tian, H. Nakayama, X.-F. Jin, and E. Saitoh, Phys. Rev. Lett. **110**, 067207 (2013).

[35] S. M. Rezende, R. L. Rodríguez-Suárez, R. O. Cunha, A. R. Rodrigues, F. L. A. Machado, G. A. Fonseca Guerra, J. C. Lopez Ortiz, and A. Azevedo, Phy. Rev. B **99**, 014416 (2014).

[36] S. M. Rezende, R. L. Rodríguez-Suárez, and A. Azevedo, Phys. Rev. B **88**, 014404 (2013).

[37] J.-C. Rojas-Sánchez, N. Reyren, P. Laczkowski, W. Savero, J.-P. Attané, C. Deranlot, M. Jamet, J.-M. George, L. Vila, and H. Jaffrès, Phys. Rev. Lett. **112**, 106602 (2014).

[38] R. W. Damon and J. R. Eshbach, J. Phys. Chem. Solids **19**, 308 (1961).

[39] S. M. Rezende and A. Azevedo, Phys. Rev. B **44**, 7062 (1991).

[40] M. J. Hurben and C. E. Patton, J. Magn. Magn. Mater. **139**, 263 (1995).

[41] S. M. Rezende, R. L. Rodríguez-Suárez, M. M. Soares, L. H. Vilela-Leão, D. Ley Domínguez, and A. Azevedo, Appl. Phys. Lett. **102**, 012402 (2013).

[42] B. Heinrich, C. Burrowes, E. Montoya, B. Kardasz, E. Girt, Y-Y. Song, Y. Sun, and M. Wu, Phys. Rev. Lett. **107**, 066604 (2011).

[43] A. Azevedo, L. H. Vilela Leão, R. L. Rodríguez-Suárez, A. F. Lacerda Santos, and S. M. Rezende, Phys. Rev. B **83**, 144402 (2011).

[44] O. Mosendz, V. Vlaminck, J. E. Pearson, F. Y. Fradin, G. E. Bauer, S. D. Bader, and A. Hoffmann, Phys. Rev. B **82**, 214403 (2010).

[45] A. Hoffmann, IEEE Trans. Magn. **49**, 5172 (2013).

[46] Y. Lamy and B. Viala, IEEE Trans. Magn. **42**, 3332 (2006).

[47] L. Liu, C.-F. Pai, Y. Li, H. W. Tseng, D. C. Ralph, and R. A. Buhrman, Science **336**, 555 (2012).